atmosphere

Article

Study on Characteristics Optimization of Combustion and Fuel Injection of Marine Diesel Engine

Guixin Wang [1], Wenbin Yu [2,*], Zining Yu [3] and Xiaobo Li [1]

[1] College of Power and Energy Engineering, Harbin Engineering University, Harbin 150001, China
[2] School of Energy and Power Engineering, Shandong University, Jinan 250061, China
[3] School of Mechanical Engineering, Tianjin University, Tianjin 300072, China
* Correspondence: wbyu@sdu.edu.cn

Highlights:

- Compared with discharge valve chamber volume, high-pressure tubing diameter shows more influence on injection mass and SMD.
- The opening pressure of needle valve is more sensitive to SMD.
- An overall simultaneous reduction of pollutant emissions was obtained, alleviating the trade-off relations between NO and soot emissions.
- Reasonable optimization of spray angle can improve power, economy and emission performance simultaneously.

Abstract: The emission requirements of diesel engines are becoming increasingly strict and reducing emissions has become the key technology. In view of this development trend, the influence law of fuel injection on emission is studied in this paper. Numerical studies were performed to analyze the structural parameters of fuel injection system on combustion and emission characteristics of marine diesel engines. The numerical modelling was validated based on single-cylinder diesel engine tests and fuel injection tests. After investigating the single structural parameters on the fuel injection characteristics, the orthogonal method was used to design the double-parameter structural optimization scheme of the fuel injection system. There are 22 optimized cases selected to further investigate using the CFD method by visualizing scalar distributions in cylinder, which was helpful to explain the reason of pollutant formation. Comprehensively comparing the performance of each fuel injection system's structural optimization scheme, moderate reduction of the discharge valve chamber volume and high-pressure tubing diameter would increase injection mass, along with faster injection rate and boosted injection pressure, leading to reduced Sauter mean diameter (SMD). Considering pollutant emission characteristics as well as economic and power concerns, case D6 with spray angle enlarging 5° showed best performance. Compared with the original condition, there was no NO deterioration and large reduction of soot emission by 65.4%, along with fuel consumption being lowered by 2.18% and more indicated power, by 2.21%. Therefore, reasonable optimization of spray angle can improve power, economy and emission performance simultaneously.

Keywords: diesel engine; fuel injection system; combustion characteristics; orthogonal method; test study

Citation: Wang, G.; Yu, W.; Yu, Z.; Li, X. Study on Characteristics Optimization of Combustion and Fuel Injection of Marine Diesel Engine. *Atmosphere* **2022**, *13*, 1301. https://doi.org/10.3390/atmos13081301

Academic Editor: Jaroslaw Krzywanski

Received: 11 July 2022
Accepted: 15 August 2022
Published: 16 August 2022

1. Introduction

In the present study, regardless of today's high supercharged diesel engine or high-pressure fuel injection diesel engine, fuel injection rate and structural parameters of fuel injection system plays an irreplaceable role in diesel engine fuel-air mixing, combustion and emission. In recent years, related research work has been carried out on the fuel injection system of high-power diesel engines. For example, Parlak et al. [1] proposed an artificial neural network model to predict specific fuel consumption and exhaust temperatures of diesel engines for various injection timings. It is considered that a well-trained neural network model provides fast and consistent results. Velez Godino et al. [2] explored methods with a late direction injection system to reduce both the engine's carbon footprint and emission of nitrogen oxides and soot, without decreasing performance or using expensive emission post-treatment systems. Shi Z et al. [3] proposed that the injection pressure effect is highly sensitive to temperature, and increased injection pressure helps optimize combustion at high temperatures but causes ignition instability at low temperatures. Wu T et al. [4] revealed that the late-injection strategy (close after main-injection) of common-rail diesel engine is capable of enhancing combustion turbulence and reducing particulate matter (PM) emissions. Khatamnejad, H. et al. [5] investigates the effect of injection pressure and double injection of diesel fuel on combustion and emissions in a reactivity-controlled compression ignition (RCCI) engine. The results indicate that high injection pressure of diesel fuel injection improves combustion features, which consequently decreases the amount of unburned hydrocarbon (HC) and carbon monoxide (CO) emissions. Srivastava, A et al. [6] found that the effect of injection pressure on the performance, emission, and combustion characteristics of a diesel-acetylene fuelled single cylinder diesel engine. Experimental results showed that highest brake thermal efficiency of 27.57% was achieved at injection pressure of 200 bar for diesel-acetylene dual-fuel mode which was much higher than 23.32% obtained for baseline diesel. These innovative studies have laid a good foundation for quantitative analysis and performance optimization of high-power diesel engine.

On the other hand, relevant researchers have also investigated the effect of combustion characteristics on diesel engine performance, fuel-air mixing and emissions. For example, Stan, L et al. [7] found that the combustion process that takes place inside of the naval diesel engines is the critical factor for determination of the level of pollution and emissions. The efficiency of such an engine is closely linked of the quality of the combustion process. Najafi, G [8] revealed that by adding nano additives to diesel–biodiesel blends, peak pressure of in-cylinder gases and the peak pressure rise rate increase in comparison with neat diesel fuel due to the shorter ignition delay resulting in earlier combustion duration and higher maximum cylinder pressure. Dev, Shouvik et al. [9] found that the reduction of engine-out NOx emissions to ultra-low levels is facilitated by enabling low temperature combustion strategies. However, there is a significant energy penalty in terms of combustion efficiency as evidenced by the high levels of hydrocarbon, carbon monoxide and hydrogen emissions. Yasuda K [10] proposed a diesel combustion model with less calculation loads that were ultimately developed with the aim of implementing such model-based controllers for engine control unit. Kapitza, L et al. [11] presented a procedure based on singular value decomposition in order to filter out measurement errors and to obtain information about the transient behavior of the in-cylinder.

Based on the above research background, the core theory of fluid dynamic and heat transfer organized by fuel injection system and combustion system is the main subject to explore, thus it is challenging to explore their synergy effects on power and economy performance, as well as emissions characteristics of diesel engines [12]. Due to the complexity of the diesel engine combustion phenomenon, comprehensive analyses based on both experimental and numerical studies are necessary. In this way the improved combustion performance could be explained and achieved by combining the advantages of each system [13,14]. In the present study, the investigations of synergy effects of each system on diesel engine performance were conducted based on a high-power diesel engine. The overall schematic of the research plan is shown in Figure 1, by using CFD numerical analysis, the fluid dynamic and heat transfer during the fuel injection, mixing and combustion process are revealed. Meanwhile, the experimental research including single cylinder engine test are designed and attached to further validate the accuracy and rationality of the numerical analysis.

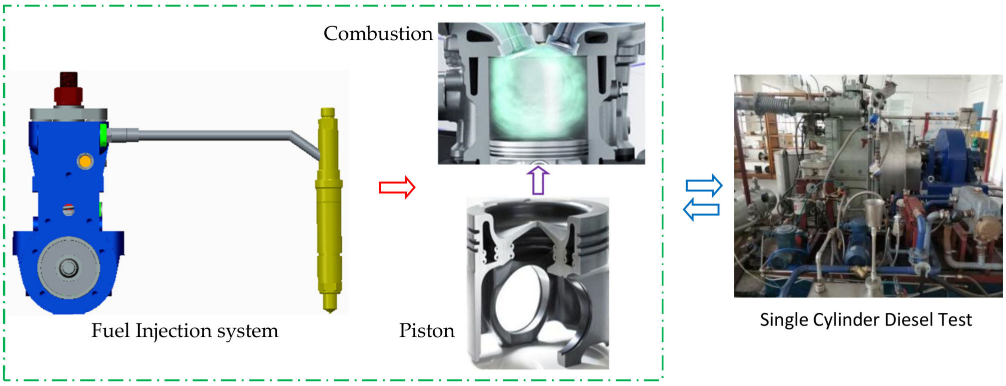

Figure 1. The overall schematic of research plan of fuel injection on combustion.

2. Results and Discussion

In order to validate the accurate of numerical modelling used to simulate diesel engine combustion in this study, experimental studies were carried on based on a single-cylinder diesel engine test bench as shown in Figure 2. The test system includes a single-cylinder diesel engine, intelligent control system and auxiliary system. The main equipment involves a Y880 hydraulic dynamometer, weighing type fuel consumption meter, flowmeter and all necessary pressure and temperature sensors etc. The objective is to study the main structure parameters of fuel system on combustion performance. The measurement results and simulation results under rated conditions are listed in Table 1 and Figure 3.

Figure 2. Single cylinder diesel engine test system.

Table 1. Comparison of simulation results and experimental results.

Performance Index	Simulation Results	Experimental Results	Relative Error
Max in-cylinder pressure	17.46 MPa	17.26 MPa	1.16%
Crank angle @ max in-cylinder pressure	6° ATDC	11° ATDC	-
Max in-cylinder temperature	1803.48 K	1850.53 K	2.54%
Crank angle @ max in-cylinder temperature	16° ATDC	20° ATDC	-
Max in-cylinder temperature before the exhaust valve is opened	1156.79 K	1201.86 K	3.75%

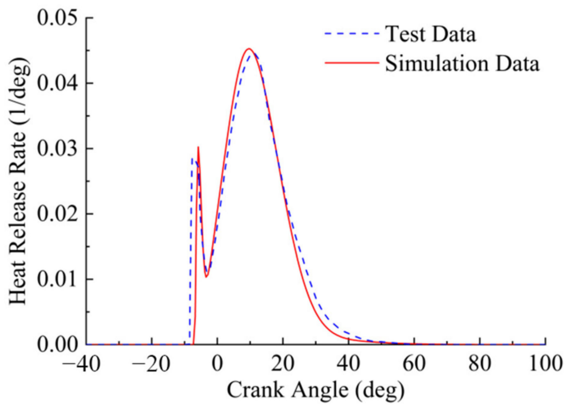

Figure 3. Comparison of heat release rate.

As listed in Table 1, the measured maximum in-cylinder pressure was 17.26 MPa, while the simulated result was 17.46 MPa with error of 1.16%. The measured maximum in-cylinder temperature was 1850.53 K, while the predicated one was 1803.48 K with error of 2.54%. Before the exhaust valve is opened, the temperature in the cylinder reaches 1156.79 K with error of 3.75%. It was found that the numerical modelling used in this study was able to predict the combustion process with acceptable tolerance. Figure 3 is the comparison of the combustion heat release rate curve. It can be seen that the curve of heat release rate obtained by simulation is in good agreement with the test data. The calculated peak value is 0.045/deg, the experimental peak value is 0.044/deg, so the relative error of the peak value of the curve is 1.7%, which is within the allowable error range.

The fuel injection test was conducted on the fuel injection test bench. The fuel injection test bench is shown in Figure 4. The main components of the test bench include a fuel pump test bench, single cylinder high pressure fuel pump, constant pressure delivery valve, high pressure fuel pipe, fuel injector, the injection flow meter, pressure sensor and EFS data collection system. The performance parameters such as pump pressure, injector pressure and injection mass were measured to validate the accuracy of the simulation model. Shown in Table 2, the maximum test pump pressure is 93.31 MPa and the maximum calculated pressure by the one-dimensional simulation model is 98.07 MPa. The relative error is 5.1%. The maximum test injector pressure is 104.11 MPa, and the maximum calculated pressure is 109.82 MPa. The relative error is 5.48%. The test value of the cumulative fuel injection volume is slightly lower than the calculated one, and the relative error is 5.26%. Based on the comparison of the above three indicators of pump pressure, injector pressure and injection mass, it is concluded that the simulation model of fuel injection system established in this study would reflect the main features of fuel spray phenomenon, so that this numerical model could be used for further optimization design and analysis on fuel injection system.

Figure 4. Fuel injection test bench.

Table 2. Fuel injection system calculation and test data.

Performance Index	Pump Pressure	Injector Pressure	Injection Mass
Calculated value	98.07 MPa	109.82 MPa	0.44 g
Test value	93.31 MPa	104.11 MPa	0.418 g
Relative error	5.1%	5.48%	5.26%

2.1. Performance of Structures of Fuel Injection System on Spray Characteristics

Optimizations of the structures of pump-tube-fuel injector system of a heavy-duty diesel engine are primarily carried on in this study [15,16], based on numerical modules of fuel injection system using AVL-Hydsim software. The numerical module of the fuel injection pump is composed of cam, plunger cavity, assemblies and leakage, inlet and outlet oil hole along with pressure boundaries. The equal pressure delivery valve module mainly includes delivery valve, return valve and delivery valve chamber. The injector module has pressure chamber, needle valve, mechanical boundary, needle valve leakage, accumulator chamber and inlet channel. The main specifications of each module are given in Table 3.

Table 3. The main configurations of injection system module.

Name	Data Input	Parameters	Name	Data Input	Parameters
Cam	Base circle diameter	40 mm	Return valve	Return valve lift	4.1 mm
	Roller diameter	28 mm		Ball valve diameter	3.5 mm
	Young's modulus	210 GPa	High-pressure pipe	Pipeline inner diameter	2.4 mm
Plunger	Moving parts weight	423 g		Pipe length	700 mm
	Plunger diameter	15 mm	Injector	Needle valve lift	0.4 mm
	Cam chamber pressure	0.1 MPa		Number of nozzles	5
	Full stroke	13 mm		Nozzle diameter	0.48 mm
	Plunger spring preload	300 N		Nozzle length	1.6 mm
Delivery valve	Delivery valve lift	5.8 mm		Moving parts weight	24.7 g
	Valve seat diameter	8.5 mm		Nozzle spring preload	1000 N

2.1.1. Fuel Spray Characteristics

The curves of fuel injection rate and cumulative injection mass are presented in Figure 5. The typical "boot type" injection starts at −20° ATDC, and rapidly rises up to maximum injection rate of 0.0524 g/deg at −3° ATDC. Then the injection rate drops rapidly and goes to zero near 5° ATDC with a short pulse caused by fluctuations of the needle valve chamber pressure. The same trend happens on the injection pressure curve, as shown in Figure 6. The injection pressure goes up rapidly after injection, starting at −20° ATDC, and reaches maximum pressure of 100.07 MPa at −3° ATDC. The simulated time-sequence Sauter Mean Diameter (SMD) of fuel spray droplets at the injector outlet is given in Figure 7. After the outset of fuel injection, the SMD quickly goes up to 21.90 μm and varies between 16 μm–18 μm during the injection process as the injection pressure increasing. Finally, to the end of fuel injection, the SMD increases to approximate 30 μm as the injection pressure dropping.

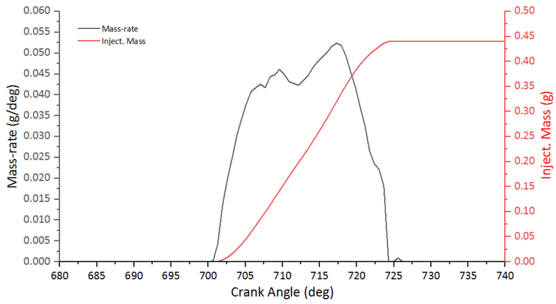

Figure 5. Curves of fuel injection rate and cumulative injection mass.

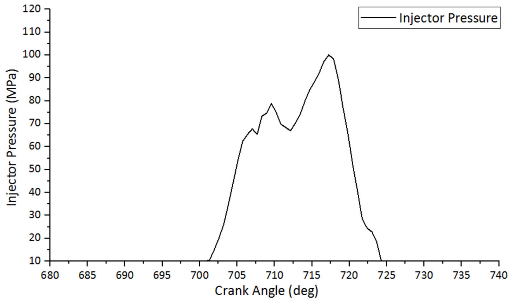

Figure 6. Curve of fuel injection pressure.

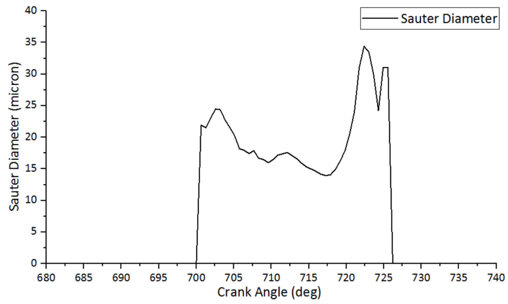

Figure 7. Sauter Mean Diameter (SMD) of fuel spray droplet.

2.1.2. Performance of Diameters of High-Pressure Oil Pipe on Spray Characteristics

When designing the fuel injection system, shortening the length of the high-pressure oil pipe is expected to boost injection pressure due to reduced pressure volume [17,18]. Therefore, the numerical modelling is used to investigate the performance of diameters of high-pressure oil pipe on spray characteristics, which are not easily realized by experimental layouts.

Five cases with diameters of 2.0 mm, 2.2 mm, 2.4 mm (base), 2.6 mm and 2.8 mm are considered. As shown in Figure 8, as the increasing of high-pressure oil pipe diameter, the fuel injection mass per cycle is reduced from 0.49 g to 0.40 g. Figure 9 gives the curves of fuel injection rate under varied diameters, and it is found the rate is going to be decreased as the diameter increases, which implies that the boosting effect of high-pressure oil pipe is limited by the pipe geometry. However, the varied diameters do not affect the onset of fuel injection too much; incremental rate of fuel injection rate and pressure is similar among all schemes as shown in Figures 9 and 10. During $-15°$ ATDC to $5°$ ATDC, the differences between varied pipe diameters are becoming clear, and the injection rate and pressure are decreasing as the diameter increases. The smallest pipe corresponds to highest pressure, leading to tiny fuel droplets. But as the diameter decreases, taking diameter of 2.0 mm as example, as shown in Figure 11, the poor pressure stabilization resulting from the boosted injection pressure causes serious pressure fluctuations at the end of injection. The injection behavior is not acceptable as the needle valve flutters and cannot be seated quickly.

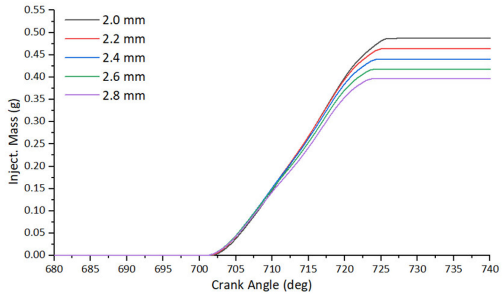

Figure 8. Cumulative fuel injection mass per cycle under varied pipe diameters.

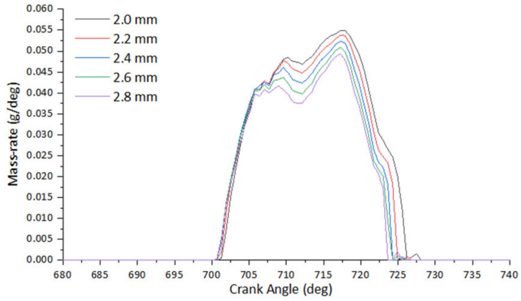

Figure 9. Fuel injection rate under varied pipe diameters.

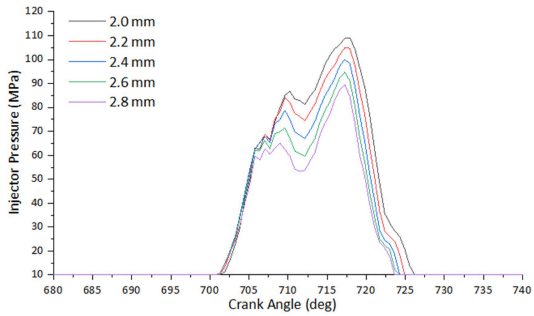

Figure 10. Fuel injection pressure under varied pipe diameters.

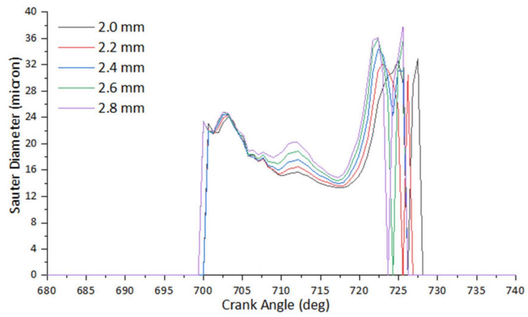

Figure 11. Fuel SMD under varied pipe diameters.

2.1.3. Performance of Initial Volume of Fuel Outlet Valve on Fuel Spray Characteristics

The volume of the fuel outlet valve plays an important role on the high-pressure fuel circuit, thus influencing the fuel injection system performance [19,20]. Five cases with 1300 mm^3, 1600 mm^3, 1950 mm^3 (base), 2400 mm^3 and 2700 mm^3 are numerically investigated to evaluate the spray characteristics.

In Figure 12, the cumulative injected fuel mass per cycle is given under varied valve volumes, and the fuel mass shows a decrease from 0.452 g to 0.427 g when the volume expands. The fuel injection rate and pressure are depicted in Figures 13 and 14. As the valve volume shrinks to 1300 mm^3, the peak of the injection rate climbs to 0.055 g/deg, which suggests an inverse relation between valve volume and injection rate peak. Moreover, one of the benefits of shrinking valve volume is the fast fuel cut-off by rapid drop of fuel injection rate. As shown in Figure 14, as the valve volume increases from 1300 mm^3 to 2700 mm^3, the peak of injection pressure decreases from 108.34 MPa to 90.22 MPa. The effects of valve volumes on fuel SMD during the injection process are compared in Figure 15. For the smallest volume of 1300 mm^3, the largest SMD of 37.6 μm appears at 5.6° ATDC and the smallest SMD of 13.34 μm happens at −2.8° ATDC. Among all studied cases, the base case of 1950 mm^3 valve volume performs best without obvious needle valve pulsation and the largest SMD is only 31.04 μm.

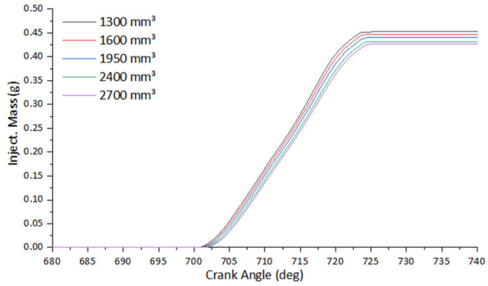

Figure 12. Cumulative fuel injection mass per cycle under varied valve volumes.

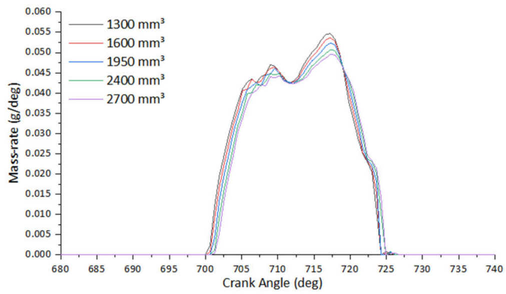

Figure 13. Fuel injection rate under varied valve volumes.

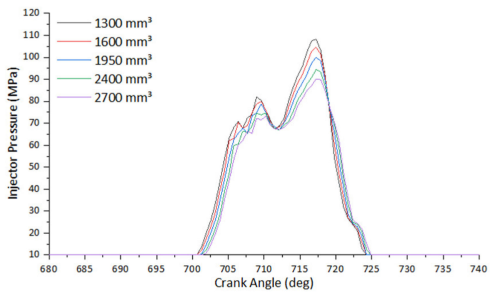

Figure 14. Fuel injection pressure under varied valve volumes.

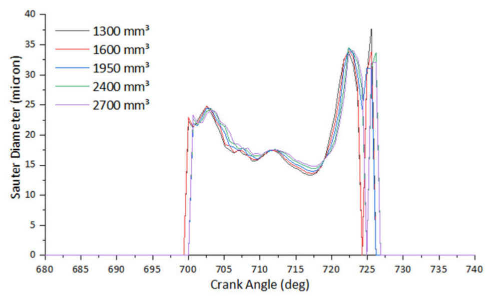

Figure 15. Fuel SMD under varied valve volumes.

2.1.4. Performance of Needle Valve Opening Pressure on Fuel Spray Characteristics

The pressure on the needle valve affects the open and close timings of the needle valve, thus influencing the fuel supply behavior [21]. With boosted needle valve opening pressure, the spray atomization could be improved during fuel injection process, and the phenomenon of secondary injection and gas flow back into the nozzle could be effectively prevented [22,23]. This paper intends to adjust the opening pressure of the needle valve by adjusting the precompression of the spring, and the investigations of fuel spray characteristics are carried on under five cases with needle valve opening pressures of 800 N, 900 N, 1000 N (base), 1100 N and 1200 N.

Figure 16 shows the cumulative injected fuel mass per cycle under varied needle valve opening pressures, as the pressure raises from 800 N to 1200 N, the fuel mass decreases from 0.47 g to 0.42 g, while the peak of injection rate drops from 0.054 g/deg to 0.049 g/deg as given in Figure 17. The higher the needle valve opening pressures, the better the performance shown at the end of fuel injection without pulse. In addition, as the needle valve opening pressures increases, the peak of the injection pressure drops from 107.73 MP to 90.72 MPa, along with retarded injection onset and shortened duration. As seen from Figure 18, it is clear that with boosted needle valve opening pressures, the secondary injection pules could be prevented.

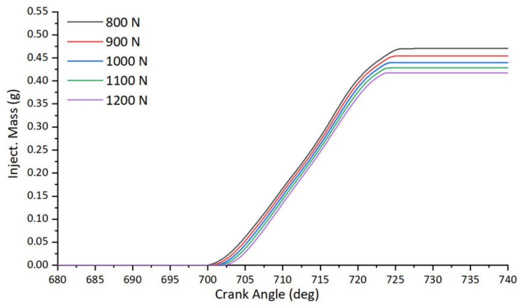

Figure 16. Cumulative fuel injection mass per cycle under varied needle valve opening pressures.

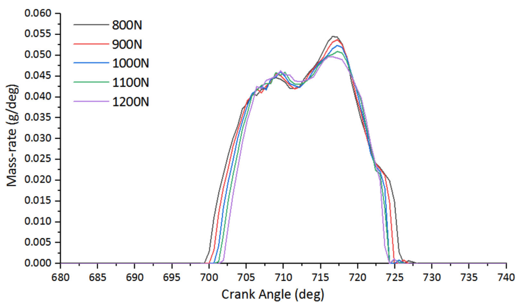

Figure 17. Fuel injection rate under varied needle valve opening pressures.

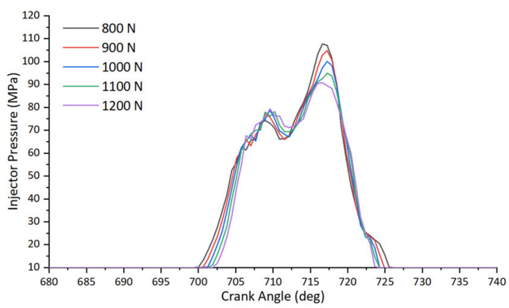

Figure 18. Fuel injection pressure under varied needle valve opening pressures.

Figure 19 shows the case with opening pressure of 800 N, the average SMD during injection fluctuation goes up to 46 μm, while the average SMD is only 29 μm for the case of 1200 N, which implies better spray atomization and lower soot formation tendency.

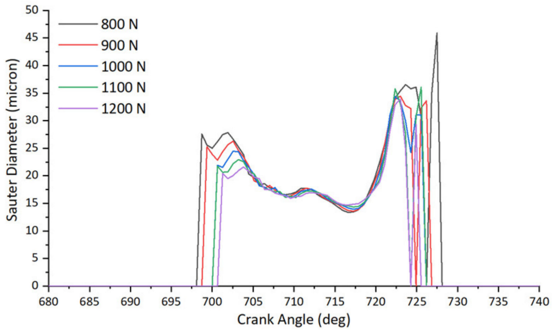

Figure 19. Fuel SMD under varied needle valve opening pressures.

2.1.5. Performance of Nozzle Diameters on Spray Characteristics

In this sector, seven cases of varied nozzle diameters are studied with diameters of 0.53 mm, 0.48 mm (base), 0.44 mm, 0.40 mm, 0.37 mm, 0.34 mm and 0.32 mm. And the length of injector nozzle remains unchanged, with corresponding length-to-radius ratio of 3.00, 3.33 (base), 3.67, 4.00, 4.33, 4.67 and 5.00.

As shown in Figures 20 and 21, the cumulative fuel injection mass and injection rate are quite sensitive to nozzle diameters. As the nozzle diameter is reduced from 0.53 mm to 0.32 mm, the fuel mass is also decreased from 0.486 g to 0.258 g and the peak of the injection rate is reduced from 0.059 g/deg to 0.028 g/deg, but with the disappearing of needle valve seat instability. It can be seen from Figure 22, that there is little effect of nozzle diameters on injection onset, but the ending of fuel injection moves forward as the nozzle diameter increases, which causes injection pressure decrease from 143.82 MPa to 86.31 MPa. During the main injection period, the fuel SMD is changing directly with nozzle diameters as shown in Figure 23, but at the end of injection, the cases with diameter of 0.32 mm and 0.34 mm lead to poor depressurization ability, which results in higher SMD at 49.27 μm for the case of 0.32 mm.

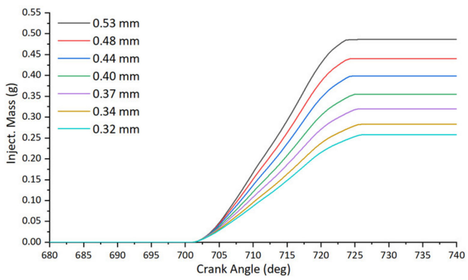

Figure 20. Cumulative fuel injection mass per cycle under varied nozzle diameters.

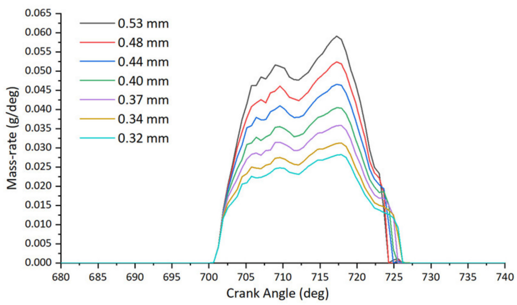

Figure 21. Fuel injection rate under varied nozzle diameters.

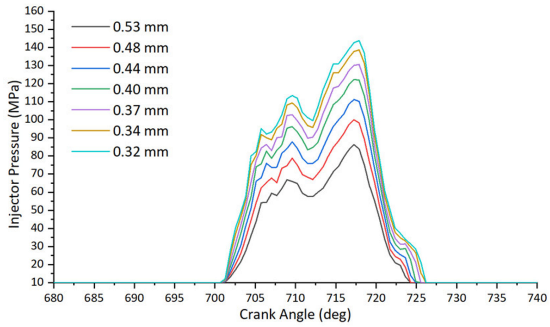

Figure 22. Fuel injection pressure under varied nozzle diameters.

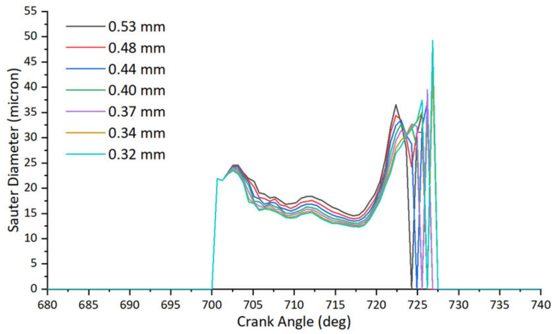

Figure 23. Fuel SMD under varied nozzle diameters.

2.2. Optimization of Fuel Injection System Based on Orthogonal Optimization Method

This study aims at optimizing fuel efficiency and emission performance of diesel engine by Structural optimization design of fuel injection system. Orthogonal optimization method is applied on dual parameter optimization designs of fuel injection system based on CFD numerical studies.

2.2.1. Orthogonal Optimization of Needle Valve Opening Pressure and Nozzle Diameter on Spray Characteristics

In this study, nine cases of nozzle diameter from 0.44 mm to 0.52 mm are considered, with five options of needle valve opening pressure from 800 N to 1200 N. After orthogonal optimization, there are 45 injector structure design schemes, and their effects on spray characteristics, predicted by Hydsim software, are plotted in Figure 24, where x-axis stands for nozzle diameter and y-axis is needle valve opening pressure, and colored contours represents each fuel injection characteristic index.

Figure 24 shows the results of fuel injection mass per cycle, with two dash line limiting $\pm$2% variation. It is found these two parameters play similar role on fuel injection mass, which trends to decease as the increasing of nozzle diameter and needle valve opening pressure. Same trending happens on the results of max injection pressure. The maximum SMD and time average SMD are also stated in Figure 24 respectively, which indicate nozzle diameter has little effect on SMD. With increasing needle valve opening pressure, SMD shows a clear decreasing trend. After considering all above phenomena and fuel injection variation limitations, the optimized structure of the fuel system is given in Table 4.

Figures 25–28 plot the curves of injection mass, injection rate, injection pressure and SMD of optimized pre-schemes in Table 4, respectively. Scheme B7 has faster injection rate with retarded injection start timing but shortened duration. Scheme B1 has earliest injection timing but with longest duration. But B1 performs higher injection pressure up to 116.69 MPa. B9 has the lowest peak of injection pressure at only 80 MPa. Meanwhile, the SMD of case B8 has the poorest injection quality, compared with B3, which keeps the lower SMD during the injection process.

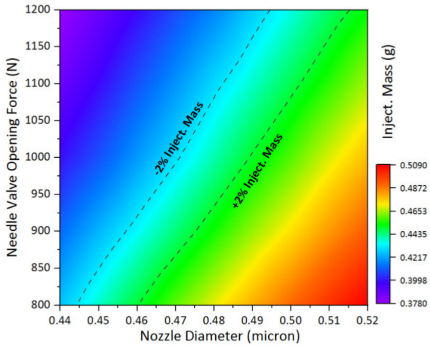

(**a**) Effect of on fuel injection mass.

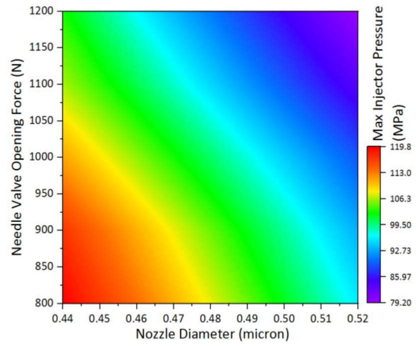

(**b**) Effect of on max fuel injection pressure.

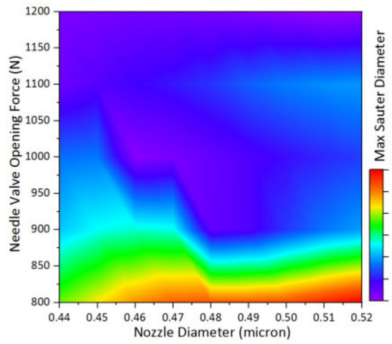

(**c**) Effect of on max SMD.

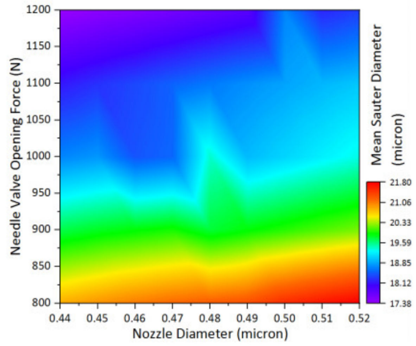

(**d**) Effect of on time-averaged SMD.

Figure 24. Effect of needle valve opening pressure and nozzle diameter on mass, pressure and SMD.

Table 4. Pre-selection scheme of fuel injector structure.

Scheme Code	B1	B2	B3	B4	B5 Original Scheme
Nozzle diameter (mm)	0.45	0.46	0.46	0.47	0.48
Nozzle valve opening force (N)	800	800	900	900	1000
Injection starting time (° CA)	698.1	698.1	698.7	698.7	700
Injection end time (° CA)	728.1	728.1	727.5	727.5	726.2
Injection mass (g)	0.438	0.449	0.434	0.444	0.440
Scheme code	**B6**	**B7**	**B8**	**B9**	
Nozzle diameter (mm)	0.49	0.50	0.50	0.51	
Nozzle valve opening force (N)	1100	1100	1200	1200	
Injection starting time (° CA)	700	700	700.6	700.6	
Injection end time (° CA)	726.2	726.2	725.6	725.6	
Injection mass (g)	0.438	0.447	0.436	0.445	

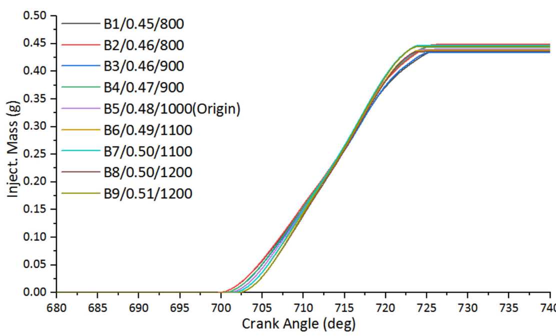

Figure 25. Cumulative fuel injection mass per cycle for Pre-selection schemes.

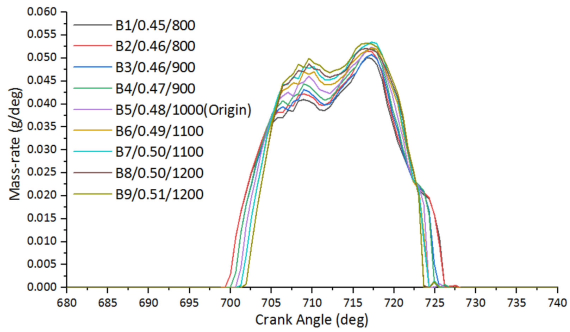

Figure 26. Fuel injection rate for Pre-selection schemes.

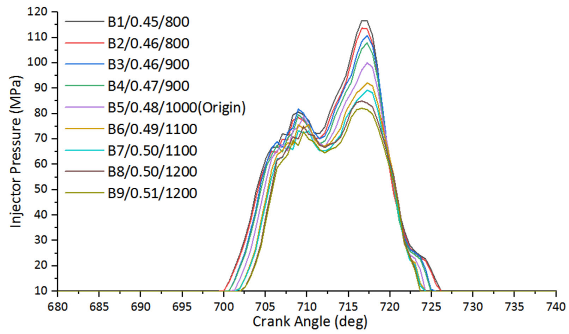

Figure 27. Fuel injection pressure for Pre-selection schemes.

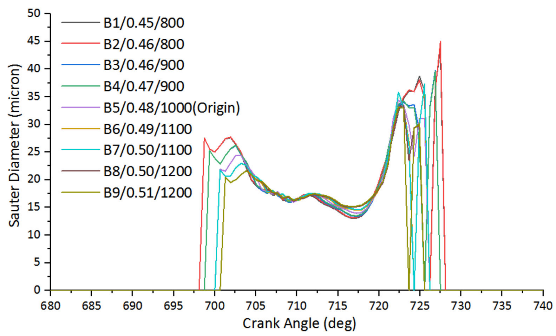

Figure 28. Fuel SMD for Pre-selection schemes.

2.2.2. Orthogonal Optimization of Diameters of High-Pressure Oil Pipe and Volume of Fuel Outlet Valve on Spray Characteristics

In this section, nine cases of diameters of high-pressure oil pipe are considered, with five options of volume of fuel outlet valve. After orthogonal optimization, there are 45 injector structure design schemes, and their effects on spray characteristics, predicted by AVL-Hydsim software, are plotted in Figure 29, where x-axis stands for diameters of high-pressure oil pipes and y-axis is fuel outlet valve volumes, and colored contours represent each fuel injection characteristic index.

Figure 29 shows the results of fuel injection mass per cycle, with two dashed lines indicating $\pm 2\%$ variation in where the injection mass is more sensitive to pip diameters. The max injection pressure increases when the valve volume is reduced. Similar trends happen, caused by pip diameters on injection pressure. The fuel SMD is more sensitive to pip diameters than valve volumes. Finally, the optimized structural of fuel system is list in Table 5.

From Figures 30–33, cases C6 and C7 have higher injection rates and peaks of injection pressure. Meanwhile C7 has earlier injection timing with shortened injection duration, but with maximum SMD due to needle lift bumping. The same conditions happen in cases C3 and C8.

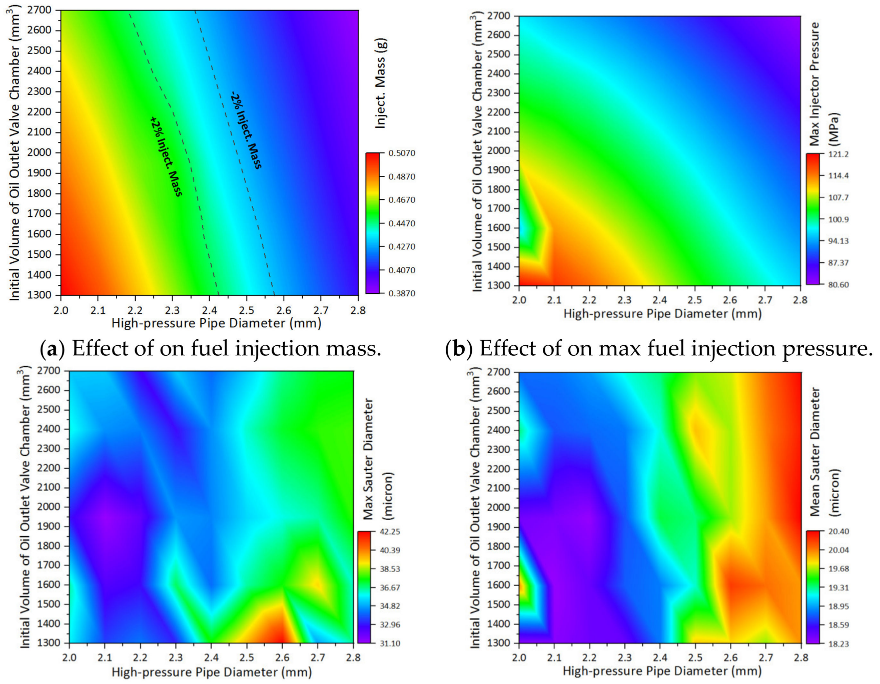

(**a**) Effect of on fuel injection mass. (**b**) Effect of on max fuel injection pressure.

(**c**) Effect of on max SMD. (**d**) Effect of on time-averaged SMD.

Figure 29. Effect of diameters of high-pressure oil pipe and volume of fuel outlet valve on mass, pressure and SMD.

Table 5. Pre-selection scheme of high-pressure volume.

Scheme Code	**C1**	**C2**	**C3**	**C4**
High-pressure pipe diameter (mm)	2.2	2.3	2.3	2.4
Initial volume of oil outlet valve chamber (mm^3)	2700	2400	2700	1600
Injection starting time (° CA)	700	700	700	699.4
Injection end time (° CA)	727.5	726.8	727.5	726.2
Injection mass (g)	0.447	0.443	0.437	0.447
Scheme code	**C5 (Origin)**	**C6**	**C7**	**C8**
High-pressure pipe diameter (mm)	2.4	2.4	2.5	2.5
Initial volume of oil outlet valve chamber (mm^3)	1950	2400	1300	1600
Injection starting time (° CA)	700	700	699.4	699.4
Injection end time (° CA)	726	726.8	726.2	726.2
Injection mass (g)	0.440	0.432	0.440	0.435

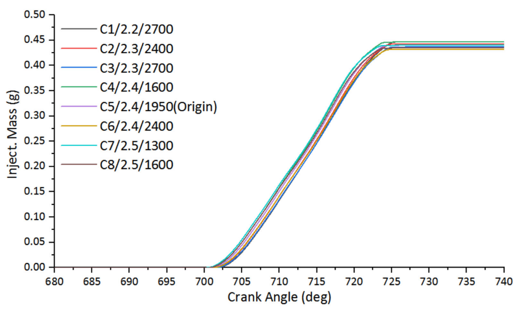

Figure 30. Volume optimization plan for injection mass.

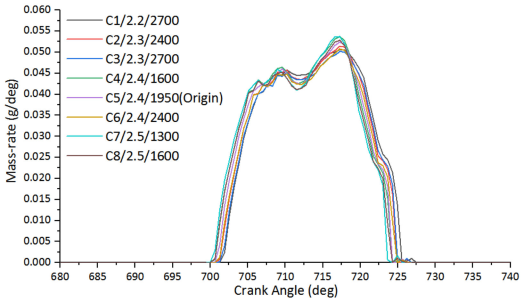

Figure 31. Volume optimization plan for mass rate.

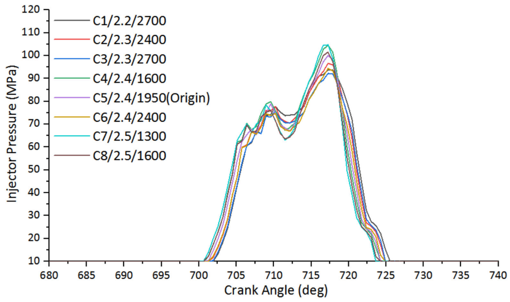

Figure 32. Volume optimization plan for injector pressure.

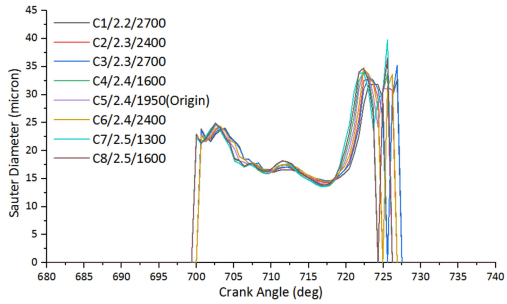

Figure 33. Volume optimization plan for SMD.

2.2.3. Orthogonal Optimization of Injector Positions and Spray Angles on Spray Characteristics

In this section, three injector positions at 3.5 mm, 4 mm (base) and 4.5 mm from combustion chamber top are considered, with three cases of spray angles of 150°, 155° (base) and 160°. There are nine injector structure design schemes after orthogonal optimization, and the layout of fuel spray is plotted in Figure 34.

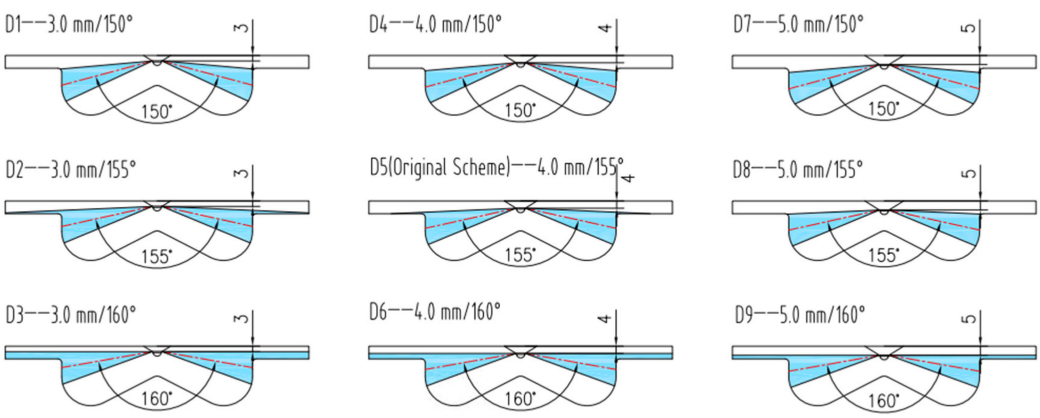

Figure 34. Different layout of injectors and spray angles.

When the spray angle is 150° (case D1, D4 and D7), the spray target is within the piston bowl, while when the spray angle extends, a few cases spray to the top clearance. In addition, when the injector orifice is further from the cylinder head, the spray target is closer to the piston bowl, as compared with case D2, D5 and D8.

2.2.4. Comparison of the Start of Injection Angle on Emissions and All Pre-Selected Schemes on Fuel Spray Characteristics

In this paper, six kinds of the start of injection angle schemes (including the original scheme) have been studied, and the combustion emission characteristics of diesel engine, shown in Table 6, have been explored. The average mass fraction of pollutants generated in the cylinder is shown in Figures 35 and 36. NO generation rate of scheme A6 is significantly higher than A1. In addition, soot also goes through the process of oxidative consumption, so it has an instantaneous peak value. The earlier the injection advance angle is, the earlier the peak time of the soot average mass fraction in cylinder arrives. The peak value of soot mass score of the original scheme in A2 is the largest among all schemes, and the maximum value is 1.56×10^{-4}, while the peak value of the soot mass score of the A6 scheme is the lowest in the whole group. In general, the more advanced the start of injection angle is, the more NO is generated in the cylinder before the exhaust valve is opened, and the lower the soot residual amount. The reason is the mixing time between fuel and air in the cylinder [24,25]. On the one hand, the more intense the fuel combustion and the higher the heat release rate, the higher the temperature in the cylinder, creating a favorable environment for NO generation. On the other hand, the formation of a soot core is effectively inhibited by more adequate in-cylinder premix.

Table 6. Scheme of the start of injection angle.

Scheme Code	Start of Injection Angle (° CA)	Injection Time (° CA)	Injection Mass (g)	Notes
A1	702	26	0.44	
A2	700	26	0.44	Original scheme
A3	698	26	0.44	
A4	696	26	0.44	
A5	694	26	0.44	
A6	692	26	0.44	

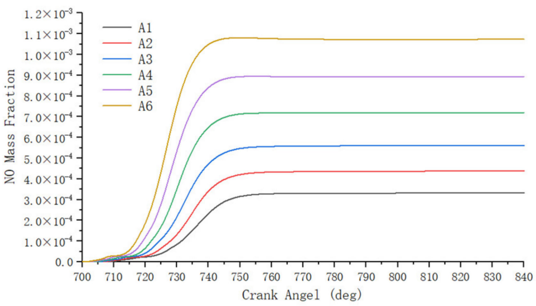

Figure 35. NO distribution of the start of injection angle.

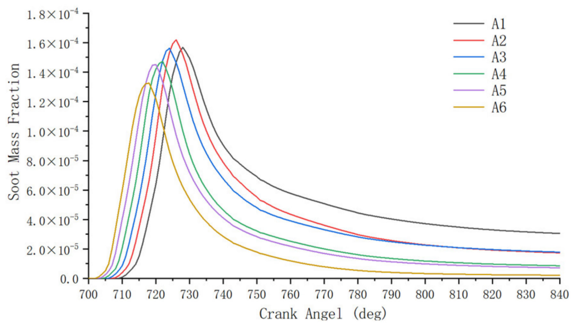

Figure 36. Soot distribution of the start of injection angle.

All optimized cases listed above are compared in Figures 37–40, and group B and C change the injector structure and high-pressure volume, thus leading to changes in spray characteristics, while group D changes the layout of spray parameters only.

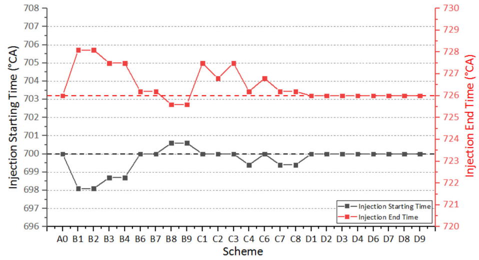

Figure 37. Injection start and end timings for each optimized case.

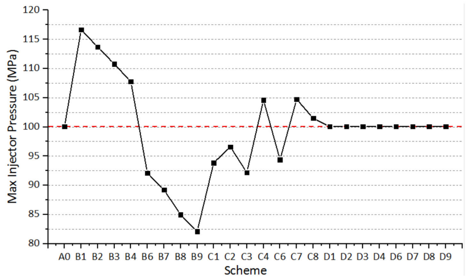

Figure 38. Max injection pressure for each optimized case.

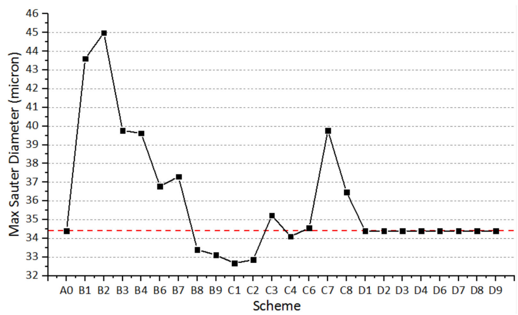

Figure 39. Max SMD for each optimized case.

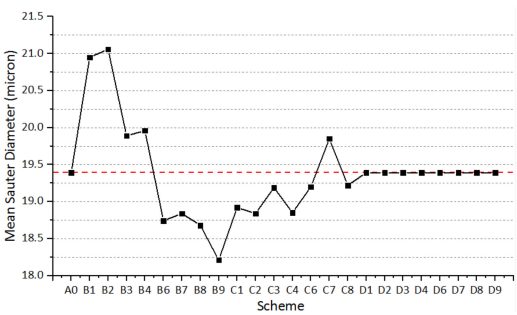

Figure 40. Time-averaged SMD for each optimized case.

In group B, B1–B4 have earlier injection timings and late injection ends, while B6 and B7 have late injection timings with earlier ends. It is deduced the onset of injection is more sensitive to needle open pressure, which causes late need lift but fast response on fuel cut-off when the needle open pressure increases. Considering the above analysis, nozzle diameters and needle valve opening pressures have similar effect on the maximum injection pressure, which is decreased as the above parameters are increased. The reason is energy loss due to increased valve opening pressure and nozzle diameter. These have an inverse effect on energy release during injection. In group B, the SMD changes directly with the nozzle diameter.

Group C targets changing the high-pressure volume of fuel injection system, wherein the maximum injection pressure is reduced as the volume is increasing. Cases C1, C2, C3 and C6 correspond to poor pressure transmission due to higher volume, leading to a delayed injection end. In the fuel injection system, fuel flows into the higher pressure pip after the outlet valve cavity, therefore the SMD is highly influenced by the pip diameter. Since C7 has the largest pip diameter, the SMD and the injection quality is the poorest.

2.3. Numerical CFD Simulation Results

In this study, AVL FIRE software is employed to numerical study diesel engine combustion and emission characteristics under optimized fuel injection system. The above selected optimized cases with better injection performance are referenced as the injection boundaries.

2.3.1. Distributions of Equivalence Ratio

The scalar fuel-air equivalence ratios in the combustion chamber are plotted in Figure 41 for selected optimized cases. At the −10° ATDC, for case B1 and C7, the main spray beam hit the bowl first, leading flame surface deformation. Because these two cases correspond with higher injection pressure (116.69 MPa, 107.74 MPa, respectively) as mentioned above, which leads to longer spray penetration and a better premixed process. For the cases of B9 and C3, with SOI at 0.6° ATDC and 0° ATDC and injection duration of 25 °CA and 27.5 °CA, they have an obvious fuel deposit remaining in the combustion chamber due to poor mixing rate in the post-combustion process [26]. At the time of 20−40° ATDC, diffusion combustion happens at the bowl bottom and top clearance. After 40° ATDC, case D6 remains at a smaller equivalence ratio which means better combustion.

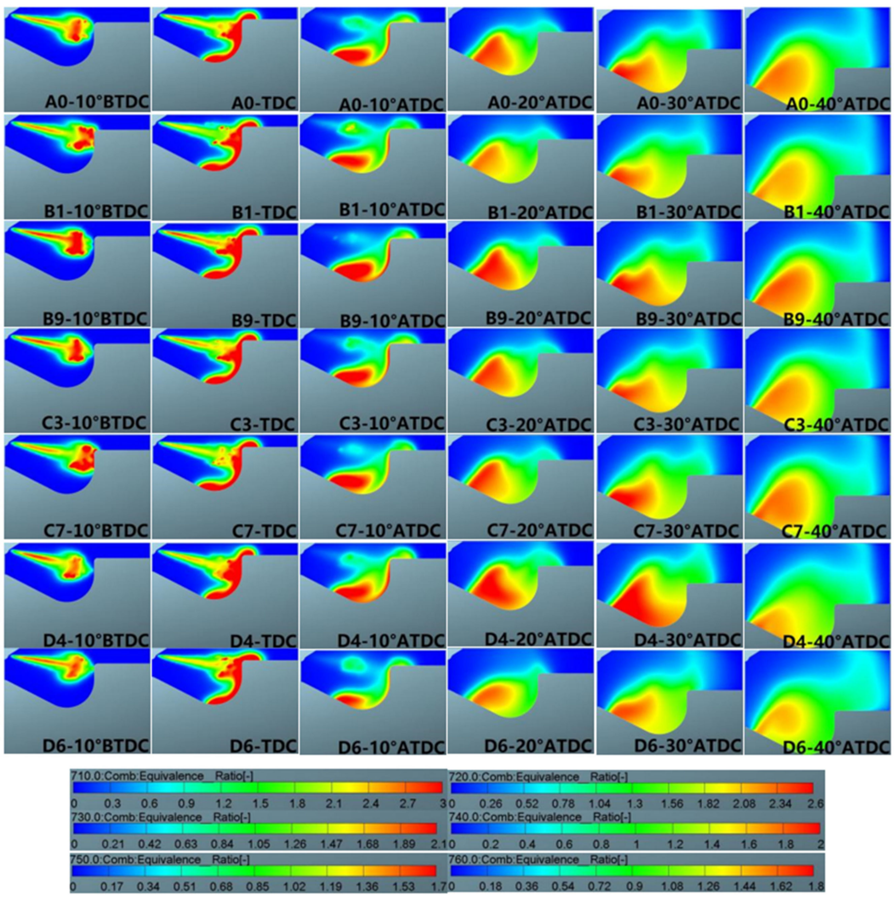

Figure 41. Distribution of equivalence ratio for pre-optimized cases.

2.3.2. Distributions of Combustion Temperature and Emissions

The scalars of temperature in the combustion chamber are plotted in Figure 42 for selected optimized cases. For cases B1 and C7, the flame surface first attaches to the chamber bowl and diffuses to a larger area, leading to a higher combustion temperature distributing into the top clearance and the piston bowl pit, as shown in Figure 42, corresponding to a higher concentration of NO distribution around the top clearance after 20° ATDC as given in Figure 43. Although higher temperature zone are located in the piston bowl pit, there is less oxygen content with higher equivalence ratio, therefore NO formation is effectively prohibited. For case B9, the maximum combustion temperature and high temperature zone area are both lower, resulting in the lowest NO emission [27,28].

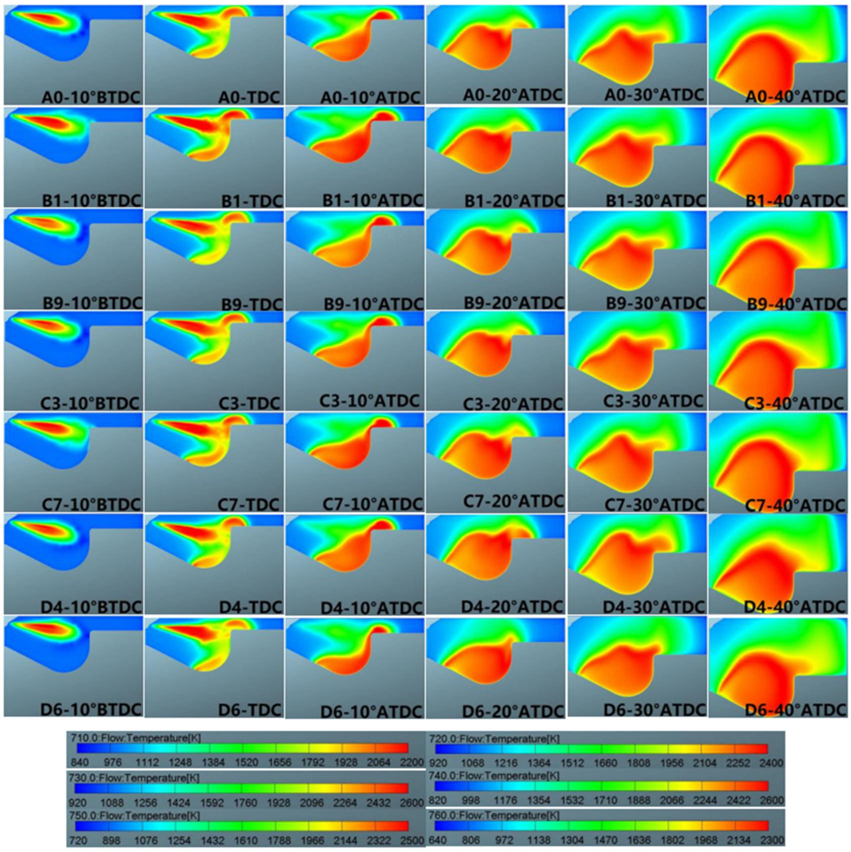

Figure 42. In-cylinder combustion temperature.

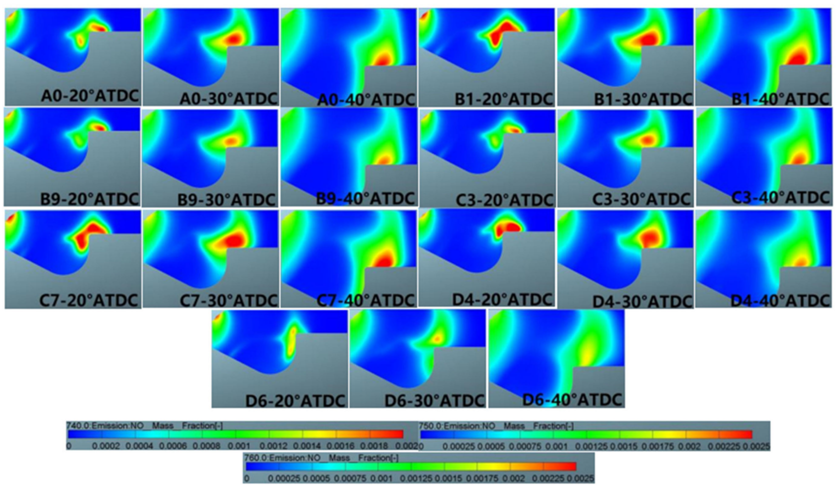

Figure 43. Map of the NO mass fraction distribution.

Soot formation is influenced, in a complicated manner, by formation rate and oxidation rate [29]. At the −10° ATDC, for cases B1 and C7 with earlier injection timing and higher injection pressure, more soot with larger area is formed, as shown in Figure 44. Moreover, due to the rich equivalence ratio along the center of the fuel spray beam and incomplete combustion, soot concentration in this area is obvious higher. At the 20–40° ATDC range, the oxidation rate of soot becomes faster than the formation rate, consuming a large amount of soot. After 40° ATDC, there is less soot remaining in the bottom of the piston bowl for case B1 and D6. Compared with the original operating conditions, B1 has a smaller injector nozzle and needle opening pressure, leading to earlier injection timing and late fuel cut-off time. D6 is designed with wider spray angle, which causes more fuel to be injected toward the piston top clearance and less deposited in the combustion bowl, accelerating the soot oxidation process, but less NO formation. While C7 has shortened fuel injection duration, which causes inadequate fuel mixing and consumption, leading soot emission was higher than the original case. Compared to D6, case D4 has smaller spray angle, leading to most of the spray beam being injected into the piston bowl. Therefore, the zone of high temperature and equivalence ratio are both located around the bottom of piston bowl, but not favoring NO formation [30]. D4 and D6 have little difference in NO emissions compared with the original case.

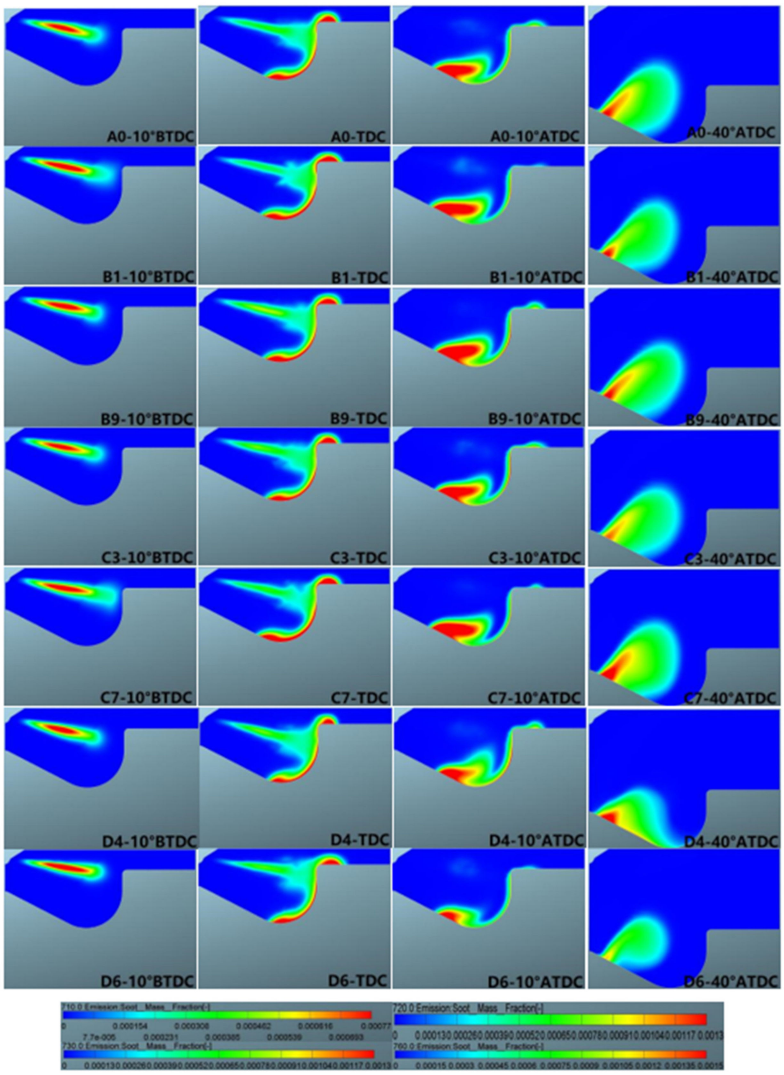

Figure 44. Map of the Soot mass fraction distribution.

2.4. Performance of Dynamic, Economy and Emission for Optimized Fuel Injection System

2.4.1. Performance of Dynamic, Economy and Emission

This section investigates the performance of dynamic, economy and emissions for above selected cases, the results are list in Figures 45–48. The fuel injection mass per cycle is controlled with variations under ±2%. Case D3 shows the best power and economy performance with injector moving up 1 mm and spray angle expending 5°. Compared with the base case, the indicated fuel consumption is reduced by 2.56% and the indicated power is increased by 2.59%. Case D4 with a shrunken 5° spray angle based on the original setup, shows a worse-performing index, with increased fuel consumption by 2.75% and decreased indicated power by 2.68%.

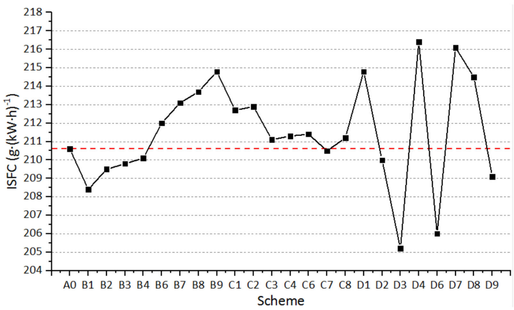

Figure 45. ISFC of each optimized design scheme.

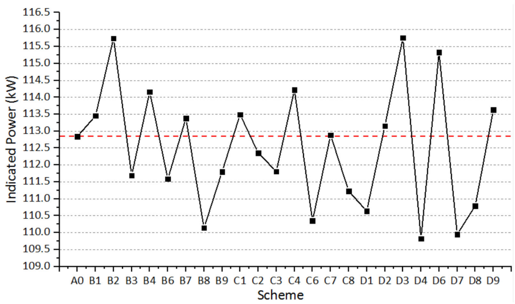

Figure 46. Indicated power of each optimized design scheme.

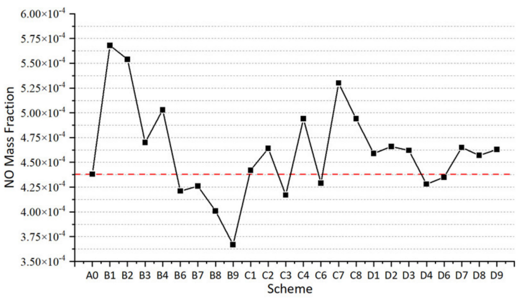

Figure 47. NO mass fraction distribution of each optimized design scheme.

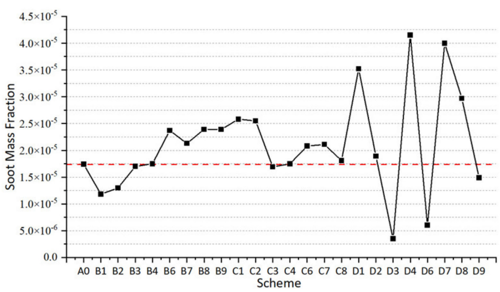

Figure 48. Soot mass fraction distribution of each optimized design scheme.

Compared with all selected cases, B9, with larger nozzle diameter and needle valve opening pressure, has lowered NO emission by 16.21%, but causes an increase in soot, by 37.36%. B1, with nozzle diameter and needle valve opening pressure lower, has poorest emissions both on NO and soot. Case D3 has the best soot emission, reduced by 52.84%, but NO emission increased by 5.71%. Case D4 has a disadvantage in soot emission, increased by 138.51%, but NO emission decreased by 2.28%. From the emission results, there are clear emission trade-off relations.

Case D6 behaves best over dynamic, economy and emissions index, with expanding 5° spray angle based on the original injector position. Compared with the original injection setup, D6 could reduce soot by 65.4% without NO increasing, while indicated fuel consumption is reduced by 2.18% and indicated power is increased by 2.21%.

2.4.2. Performance between Injection Characteristics and Emissions

For case B1–B4, with the same change of injector diameter and needle opening pressure, with advanced injection timing, the combustion temperature is obviously increased, causing higher NO formation but with lower soot emissions compared to the original case. However, increased injection pressure plays little effect on emissions without better performance on SMD but produced less soot emission.

For group C, with optimization of high-pressure volume, case C3 generate less NO and soot compared to the original case. It was caused by reduced volume of the fuel outlet valve chamber, thus smoothing pressure fluctuations in high-pressure fuel pip, which lead to smaller SMD.

Group D focuses on optimizing the spray target by changing injector axial positions and spray angles. Because fuel consumption rate is strongly dependent on turbulent flow in-cylinder during pre-combustion stage, the proper injection orientation avoids fuel deposit in the area with poor mobility, such as the piston top clearance and the bottom of the piston bowl. Case D6 performs better on the induced spray target, getting rid of rich fuel deposits, which facilitates complete combustion and soot mitigation.

3. Conclusions

In this study, one-dimensional fuel injection system simulations and three-dimensional CFD in-cylinder combustion simulations were conducted to analyze fuel injection, combustion and emission characteristics of a marine diesel engine. The numerical modelling was validated based on single-cylinder diesel engine tests and fuel injection tests. The structural parameters of the fuel injection system were improved in order to find out the key structural parameters that affect the fuel supply. Therefore, the optimized cases with reduced emissions and improved power performance were explored. The main findings are below:

(1) Moderate reduction of the discharge valve chamber volume and high-pressure tubing diameter would reduce SMD. Compared with discharge valve chamber volume, high-pressure tubing diameter shows more influence on injection mass and SMD but equal effect on injection pressure.

(2) In the orthogonal design scheme, the volume of the oil outlet valve cavity and the diameter of the high-pressure tubing are adjusted simultaneously. Case C3 performs best with both NO and soot decreased by 4.79% and 2.87, respectively.

(3) Comprehensively comparing the performance of each fuel injection system's structural optimization scheme, considering pollutant emission characteristics as well as economic and dynamic indicators, case D6 with spray angle enlarged to 5° showed the best performance. Compared with original conditions, there were no NO deteriorations and a large reduction of soot emission, by 65.4%, along with lower fuel consumption, by 2.18%, and more indicated power, by 2.21%.

Author Contributions: Conceptualization, methodology, software, writing-Original draft preparation, G.W.; Experimental analysis, investigation, data analysis, W.Y.; Writing reviewing and editing, Z.Y.; Supervision, software, validation, X.L. All authors have read and agreed to the published version of the manuscript.

Funding: This research was funded by China Scholarship Council (grant number 201706685042).

Institutional Review Board Statement: Not applicable.

Informed Consent Statement: Not applicable.

Data Availability Statement: Exclude this statement.

Acknowledgments: This work acknowledges the project of Research on Thermal Load and Heat Transfer Characteristics of High-Strength Diesel Engine.

Conflicts of Interest: The authors declared that they have no conflicts of interest to this work. We declare that we do not have any commercial or associative interest that represents a conflict of interest in connection with the work submitted.

References

1. Adnan, P.; Yasar, I.; Halit, Y.; Aysun, E. Application of artificial neural network to predict specific fuel consumption and exhaust temperature for a Diesel engine. *Appl. Therm. Eng.* **2005**, *26*, 824–828.
2. Godiño, J.A.V.; García, M.T.; Aguilar, F.J.J.E. Experimental analysis of late direct injection combustion mode in a compression-ignition engine fuelled with biodiesel/diesel blends. *Energy* **2021**, *239*, 624–637.
3. Shi, Z.; Wu, H.; Li, H.; Zhang, L.; Li, X.; Lee, C. Effect of injection pressure and fuel mass on wall-impinging ignition and combustion characteristics of heavy-duty diesel engine at low temperatures. *Fuel* **2021**, *299*, 236–247. [CrossRef]
4. Wu, T.; Yao, A.; Yao, C.; Pan, W.; Wei, H.; Chen, C.; Gao, J. Effect of diesel late-injection on combustion and emissions characteristics of diesel/methanol dual fuel engine. *Fuel* **2018**, *233*, 217–327. [CrossRef]
5. Khatamnejad, H.; Khalilarya, S.; Jafarmadar, S.; Mirsalim, M. The effect of high-reactivity fuel injection parameters on combustion features and exhaust emission characteristics in a natural gas-diesel RCCI engine at part load condition. *Int. J. Green Energ.* **2018**, *15*, 874–888. [CrossRef]
6. Srivastava, A.K.; Soni, S.L.; Sharma, D.; Jain, N.L. Effect of injection pressure on performance, emission, and combustion characteristics of diesel-acetylene-fuelled single cylinder stationary CI engine. *Environ. Sci. Pollut. Res.* **2018**, *25*, 7767–7775. [CrossRef]
7. Stan, L.C.; Memet, F.; Buzbuchi, N. Combustion simulation for naval diesel engine. *Adv. Marit. Nav. Sci. Eng.* **2010**, *3*, 57–60.
8. Najafi, G. Diesel engine combustion characteristics using nano-particles in biodiesel-diesel blends. *Fuel* **2018**, *212*, 668–678. [CrossRef]
9. Dev, S.; Divekar, P.; Xie, K.; Han, X.Y.; Chen, X.; Zheng, M. A Study of Combustion Inefficiency in Diesel Low Temperature Combustion and Gasoline-Diesel RCCI Via Detailed Emission Measurement. *J. Eng. Gas. Turb. Power* **2015**, *137*, 121501. [CrossRef]
10. Asuda, K.; Yamasaki, Y.; Kaneko, S.; Nakamura, Y.; Lida, N.; Hasegawa, R. Diesel combustion model for on-board application. *Int. J. Engine Res.* **2016**, *17*, 748–765. [CrossRef]
11. Kapitza, L.; Imberdis, O.; Bensler, H.P.; Willand, J.; Theveni, D. An experimental analysis of the turbulent structures generated by the intake port of a DISI-engine. *Exp. Fluids.* **2010**, *48*, 265–279. [CrossRef]
12. Genzale, C.L.; Reitz, R.D.; Musculus, M.P.B. Effects of Piston Bowl Geometry on Mixture Development and Late-Injection Low-Temperature Combustion in a Heavy-Duty diesel engine. *SAE* **2008**, *1*, 913–937. [CrossRef]
13. Wang, G.; Yu, W.; Li, X.; Su, Y.; Yang, R.; Wu, W. Experimental and numerical study on the influence of intake swirl on fuel spray and in-cylinder combustion characteristics on large bore diesel engine. *Fuel* **2019**, *237*, 209–221. [CrossRef]
14. Ilker, Y. Effect of swirl number on combustion characteristics in a natural gas diffusion flame. *J. Energe. Resour.* **2013**, *135*, 42–47.
15. Wang, T.; Liu, D.; Wang, G.; Tan, B.; Peng, Z. Effects of Variable Valve Lift on In-Cylinder Air Motion. *Energies* **2015**, *8*, 13779–13781. [CrossRef]
16. Kim, S.; Nouri, J.M.; Yan, Y.; Arcoumanis, C. Effects of intake swirl and coolant temperature on spray structure of a high pressure multi-hole injector in a direct-injection gasoline engine. *J. Phys.* **2005**, *85*, 45–53. [CrossRef]
17. Miles, P.C.; Megerle, M.; Nagel, Z.; Liu, Y.; Reitz, R.D.; Lai, M.C.; Sick, V. The Influence of Swirl and Injection Pressure on Post-Combustion Turbulence in a HSDI Diesel Engine. In *Thermo- and Fluid Dynamic Processes in Diesel Engines 2*; Springer: Berlin/Heidelberg, Germany, 2004; pp. 134–137.
18. Basha, S.A.; Gopal, K.R. In-cylinder fluid flow, turbulence and spray models. *Renew Sust. Energ. Rev.* **2009**, *13*, 1620–1624. [CrossRef]
19. Jayashankara, B.; Ganesan, V. Effect of fuel injection timing and intake pressure on the performance of a DI diesel engine-A parametric study using CFD. *Energ. Convers. Manage.* **2010**, *51*, 1838–1844. [CrossRef]
20. Maroteaux, F.; Saad, C. Diesel engine combustion modeling for hardware in the loop applications: Effects of ignition delay time model. *Energy* **2013**, *57*, 641–650. [CrossRef]

21. Kook, S.; Bae, C.; Miles, P.C.; Choi, D. The effect of swirl ratio and fuel injection parameters on CO emission and fuel conversion efficiency for high-dilution, low-temperature combustion in an automotive diesel engine. *SAE* **2006**, *80*, 2261–2267.
22. David, J.R.; Thathapudi, K.N.M. Studies on variable swirl intake system for DI diesel engine using computational fluid dynamics. *Therm. Sci.* **2008**, *12*, 25–32.
23. Micklow, G.J.; Gong, W.D. Intake and in-cylinder flow field modelling of a four-valve diesel engine. *Proc. Inat. Mech. Eng. Part D J. Automob. Eng.* **2007**, *221*, 1426–1435.
24. Wang, S.; Zhang, J.; Yao, L. Effect of Combustion Boundary Conditions and n-Butanol on Surrogate Diesel Fuel HCCI Combustion and Emission Based on Two-Stroke Diesel Engine. *Atmosphere* **2022**, *13*, 303. [CrossRef]
25. Selleri, T.; Melas, A.; Ferrarese, C.; Franzetti, J.; Giechaskiel, B.; Suarez-Bertoa, R. Emissions from a Modern Euro 6d Diesel Plug-In Hybrid. *Atmosphere* **2022**, *13*, 1175. [CrossRef]
26. Dembinski, H.W.R. The effects of injection pressure and swirl on in-cylinder flow pattern and combustion in a compression-Ignition engine. *Int. J. Engine Res.* **2014**, *15*, 444–459. [CrossRef]
27. Wang, F.; Xie, X.; Jiang, Q.; Zhou, L. Effect of turbulence on NO formation in swirling combustion. *Chinese J. Aeronaut.* **2014**, *27*, 797–804. [CrossRef]
28. Cheung, C.S.; Zhang, Z.H.; Chan, T.L.; Yao, C. Investigation on the effect of port-injected methanol on the performance and emissions of a diesel engine at different engine speeds. *Energe. Fuel.* **2009**, *23*, 5684–5694. [CrossRef]
29. He, X.; Tan, Q.; Wu, Y.; Wei, C. Optimization of Marine Two-Stroke Diesel Engine Based on Air Intake Composition and Temperature Control. *Atmosphere.* **2022**, *13*, 355. [CrossRef]
30. Zhu, Y.; Zhou, W.; Xia, C.; Hou, Q. Application and Development of Selective Catalytic Reduction Technology for Marine Low-Speed Diesel Engine: Trade-Off among High Sulfur Fuel, High Thermal Efficiency, and Low Pollution Emission. *Atmosphere* **2022**, *13*, 731. [CrossRef]